Available online at www.sciencedirect.com
SCIENCE DIRECT®
Journal of Solid State Chemistry 177 (2004) 3805–3814
JOURNAL OF SOLID STATE CHEMISTRY
www.elsevier.com/locate/jssc

Different crystal structure and photophysical properties of lanthanide complexes with 5-bromonicotinic acid

Song Yi-Shan[a], Yan Bing[a,*], Chen Zhen-Xia[b]

[a] *Department of Chemistry, Tongji University, Siping Road 1239, Shanghai 200092, PR China*
[b] *Department of Chemistry, Fudan University, Shanghai 200433, PR China*

Received 31 January 2004; received in revised form 7 April 2004; accepted 13 July 2004
Available online 27 August 2004

Abstract

Five novel lanthanide (Eu^{3+} (**1**), Tb^{3+} (**2**), Sm^{3+} (**3**), Dy^{3+} (**4**) and Gd^{3+} (**5**)) complexes with 5-Bromonicotinic acid (5-Brnic) were synthesized and two of them (Tb^{3+}, Sm^{3+}) were characterized by X-ray diffraction. The results reveal that $\{[Tb(5\text{-}Brnic)_3(H_2O)_3]\cdot H_2O\}_n$ (**2**) and $[Sm(5\text{-}Brnic)_3(H_2O)_2\cdot H_2O]_2$ (**3**) exhibit different coordination geometries and crystal structures. Complex **2** has a one-dimensional chain-like polymeric structure through the bridged 5-Brnic anions which links up two neighboring terbium ions, while Complex **3** forms a dimeric molecular structure. The lowest triplet state energy of 5-Brnic was determined to be 24 330 cm^{-1} corresponded to the 0–0 transition in the phosphorescence spectrum of its gadolinium complex at 411 nm. The strong luminescent emission intensities of these complexes indicated that the triplet state energy of 5-Brnic is suitable for the sensitization of luminescence of Eu^{3+}, Tb^{3+}, Sm^{3+} and Dy^{3+}, especially for that of Tb^{3+} and Dy^{3+}.

Keywords: Lanthanide complexes; Crystal structure; Photophysical properties; 5-Bromonicotinic acid

1. Introduction

In recent years, lanthanide complexes have received much attention because of their interesting photophysical properties which have potential application in the luminescence probes for chemical or biological macromolecules and the active center for luminescent materials [1–4]. And considerable studies have been focused on the design and assembly of lanthanide complexes with organic ligands such as aromatic carboxylic acids, β-diketone, cryptands, calixarenes and heterocyclic ligands, etc. Among the lanthanide complexes with aromatic carboxylic acids show higher thermal or luminescent stabilities for practical application than other lanthanide complex systems because they readily form the dimeric or infinite chain polymeric structures [5–15]. Pyridinecarboxylic acids belong to heterocyclic acids with conjugated structures and some papers have discussed the molecular or crystal structures for some lanthanide (La, Sm, Eu and Ho) ions [9–15]. In the present work, we synthesized the 5-Brnic complexes with luminescent lanthanide ions (Eu^{3+}, Tb^{3+}, Gd^{3+}, Sm^{3+} and Dy^{3+}). It is worthy pointing out that $\{[Tb(5\text{-}Brnic)_3(H_2O)_3]\cdot H_2O\}_n$ (**2**) and $[Sm(5\text{-}Brnic)_3(H_2O)_2\cdot H_2O]_2$ (**3**) exhibit different coordination geometries and crystal structures, in spite of the similar reactant and reaction conditions. The photophysical properties of these complexes were studied with ultraviolet absorption spectra, phosphorescence spectrum, fluorescence excitation and emission spectra. The detailed crystal structure and photophysical properties are discussed here.

2. Experimental part

2.1. Chemicals and physical measurements

$Ln(NO_3)_3\cdot 6H_2O$ were prepared by the corresponding lanthanide oxides (Eu_2O_3, Tb_4O_7, Gd_2O_3, Sm_2O_3,

*Corresponding author. Fax: +862165982287.
E-mail address: byan@tongji.edu.cn (Y. Bing).

0022-4596/$ - see front matter © 2004 Elsevier Inc. All rights reserved.
doi:10.1016/j.jssc.2004.07.035

Dy_2O_3) with concentrated nitric acid [16]. 5-Brnic was purchased from *Aldrich* and used without purification. Elemental analyses (C, H, N) were determined with an *Elementar Cario EL* elemental analyzer. IR spectra were recorded with a *Nicolet Nexus 912 AO446* spectrophotometer (KBr pellet), 4000–400 cm^{-1} region. Ultraviolet absorption spectra were measured using an *Agilent 8453* spectrophotometer. The phosphorescence spectrum was determined with Perkin-Elmer LS-55 spectrophotometer: excitation wavelength = 370 nm, delay time = 0.01 ms, scan speed = 1000 nm/s, and the phosphorescence measurement began 100 μs after lamp flash and it continued 200 μs. The luminescence (excitation and emission) spectra for the solid complex samples were determined with a Perkin-Elmer LS-55 spectrophotometer, whole excitation and emission slit width were 10 and 5 nm, respectively.

2.2. Synthesis of the complexes

Lanthanide oxides (Eu_2O_3, Tb_4O_7, Gd_2O_3, Sm_2O_3, Dy_2O_3) were converted to their nitrates by treatment with concentrated nitric acid according to conventional method [16]. To an aqueous (5 mL) solutions of $Ln(NO_3)_3 \cdot 6H_2O$ ($Sm(NO_3)_3 \cdot 6H_2O$, 0.222 g/0.5 mmol; $Eu(NO_3)_3 \cdot 6H_2O$, 0.223 g/0.5 mmol, $Gd(NO_3)_3 \cdot 6H_2O$, 0.226 g/0.5 mmol; $Tb(NO_3)_3 \cdot 6H_2O$, 0.227 g/0.5 mmol, $Dy(NO_3)_3 \cdot 6H_2O$, 0.229 g/0.5 mmol), 5-Bromonicotinic acid (5-Brnic, 0.3029 g/1.5 mmol) in a minimum amount of ethanol was slowly added under stirring. The pH value of the mixed solution was adjusted to be about 6.5 with sodium hydroxide and further stirred for 4 h, then a little white precipitate for the product (lanthanide complexes) appeared. The resulting solution was filtered and the filtrate allowed to standing at room temperature. After 1 week, well-shaped light colorless single crystals of complexes **2** and **3** suitable for X-rays four-circle diffraction analysis were obtained. *Data of Eu complex* (**1**): Yields: 88%. IR (main bands): 1543 ($v_s COO^-$), 1413, ($v_{as} COO^-$). Anal. Calcd. for $C_{36}H_{30}Br_6N_6O_{18}Eu_2$: C, 26.70; H, 1.85; N, 5.19; Found: C 26.47; H, 1.92; N, 5.04. *Data of Tb complex* (**2**): Yields: 85%. IR (main bands): 1543 ($v_s COO^-$), 1413, ($v_{as} COO^-$). Anal. Calcd. for $C_{18}H_{17}Br_3N_3O_{10}Tb$: C, 25.90; H, 2.04; N, 5.04; Found: C 26.43; H, 2.15; N, 4.97. *Data of Sm complex* (**3**): Yields: 89%. IR (main bands): 1543 ($v_s COO^-$), 1413, ($v_{as} COO^-$). Anal. Calcd. for $C_{36}H_{30}Br_6N_6O_{18}Sm_2$: C, 26.75; H, 1.86; N, 5.20; Found: C 26.37; H, 1.92; N, 5.07. *Data of Dy complex* (**4**): Yields: 88%. IR (main bands/cm^{-1}): 1413 ($v_s COO^-$), 1543, ($v_{as} COO^-$). Anal. Calcd. for $C_{36}H_{30}Br_6N_6O_{18}Dy_2$: C, 25.79; H, 2.03; N, 5.01; Found: C 25.43; H, 2.12; N, 4.93. *Data of Gd complex* (**5**): Yields: 82%. IR (main bands): 1543 ($v_s COO^-$), 1413, ($v_{as} COO^-$). Anal. Calcd. for $C_{36}H_{30}Br_6N_6O_{18}Gd_2$: C, 26.90; H, 1.74; N, 5.03; Found: C 26.61; H, 1.83; N, 4.89. From the estimation of elemental analysis data, the complexes of Sm, Eu and Gd ions belong to the similar composition, while those of Tb and Dy are the same composition, which is harmony with other lanthanide complexes with pyridine-carboxylic acids [9–15].

2.3. Crystal data collection and refinement (Table 1)

Diffraction experiment of a light-colorless crystal with dimensions 0.15 × 0.10 × 0.05 mm for complex (**2**) and 0.20 × 0.15 × 0.05 mm for complex (**3**) were performed with graphite-monochromated Mo$K\alpha$ radiation (λ0.71073 Å) on a CCD detector four-circle diffractometer. In total, 6282 (**2**) (11273 (**3**)) reflection intensity data were collected, of which 5292 (**2**) (5407 (**3**)) independent reflections were measured in the range $1.77 \leqslant \theta \leqslant 27.10$ (**2**) ($2.10 \leqslant \theta \leqslant 27.16$ (**3**)) at 293(2) K by the $\omega - 2\theta$ scan technique. An empirical absorption correction was applied by means of the SADABS, which gave the transmission factor: min/max 0.3937/0.7013 (**2**) (0.3060/0.6977 (**3**)). The crystal structure was solved by direct methods and *Fourier* synthesis with the program SHELXS−97 [17] and refined by the full-matrix least-squares method on F^2, with the program SHELXL−97 [18]. The function minimized was $\Sigma w(|F_o|^2 - |F_c|^2)^2$, where $w = [s^2(F_o^2) + (0.0727P)^2 + 0.0000P]^{-1}$ and $P = (F_o^2 + 2F_c^2)/3$. All non-hydrogen atoms were refined anisotropically by full-matrix least-squares methods. The whole hydrogen atoms including the water hydrogen atoms were added geometrically and not refined. In all, 340 (**2**) (331 (**3**)) parameters were refined for 5292 (**2**) (5403 (**3**)) reflections. Refinement converged at R (on F) 0.0316 (for **2**), 0.0281 (for **3**), wR (on F^2) 0.0695 (for **2**), 0.0582 (for **3**). Maximum and minimum peaks in the final difference maps were 0.851 e $Å^{-3}$ and −1.497 e $Å^{-3}$ for complex **2** and 0.834 e $Å^{-3}$ and −1.217 e $Å^{-3}$ for complex **3**, respectively.

3. Results and discussion

3.1. Crystal Structures

Fig. 1(a) and Table 1 show the coordination geometry and atom labeling in the crystal structure of complex **2**. X-ray diffraction (XRD) crystal structure analysis reveals that it leads to a one-dimensional (1-D) chain-like formulation $\{[Tb(5\text{-Brnic})_3(H_2O)_3] \cdot H_2O\}_n$ with two bridged 5-Brnic carboxyaltes connecting the two adjacent terbium ions. Fig. 1(b) shows the chain-like structure diagram of the coordination polymer, which is similar with the 1-D complex $\{[Sm(C_5H_4NCO_2)_3(H_2O)_2]_2\}_n$ we have reported [12]. Each central Tb ion belongs to eight-coordinated with eight coordinated oxygen atoms, whose coordination geometry can be described as a distorted square antiprism geometry.

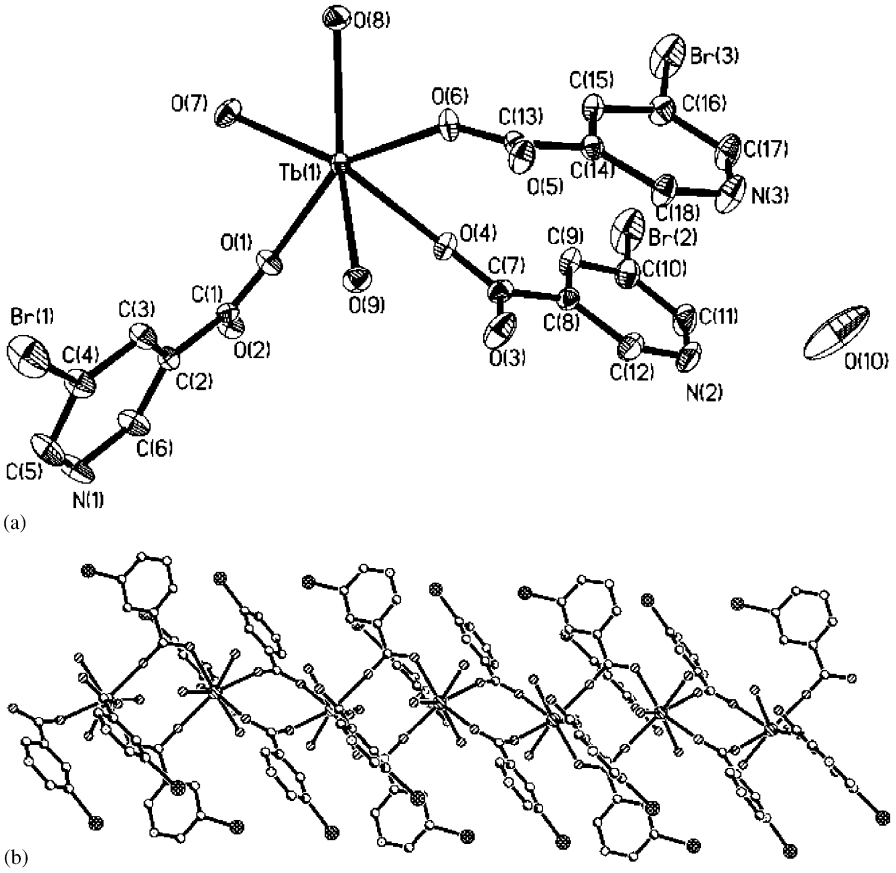

Fig. 1. Molecular structure (a) and 1-D view (b) of $\{[Tb(5\text{-}Brnic)_3(H_2O)_3]\cdot H_2O\}_n$ coordination polymer.

Table 1
Crystal data and structure refinement for $\{[Tb(5\text{-}Brnic)_3(H_2O)_3]\cdot H_2O\}_n$ and $[Sm(5\text{-}Brnic)_3(H_2O)_2\cdot H_2O]_2$

	$\{[Tb(5\text{-}Brnic)_3(H_2O)_3]\cdot H_2O\}_n$	$[Sm(5\text{-}Brnic)_3(H_2O)_2\cdot H_2O]_2$
Empirical formula	$C_{18}H_{17}Br_3N_3O_{10}Tb$	$C_{36}H_{30}Br_6N_6O_{18}Sm_2$
Relative molecular weight M	834.00	1614.82
Temperature	293(2) K	298(2) K
Wavelength	0.71073 Å	0.71073 Å
Crystal system	P_{-1}	$P2(1)/n$
Space group	Triclinic	Monoclinic
Unit dimensions	$a = 10.0741(16)$ Å	$a = 11.697(4)$ Å
	$b = 11.5506(18)$ Å	$b = 16.640(5)$ Å
	$c = 11.5642(18)$ Å	$c = 12.217(4)$ Å
	$\alpha = 88.526(2)^\circ$	
	$\beta = 85.621(2)^\circ$	$\beta = 102.819(4)^\circ$
	$\gamma = 69.490(2)^\circ$	
Volume	1256.7(3) Å^3	2318.6(12) Å^3
Z	2	2
Calculated density	2.204 Mg/m^3	2.313 Mg/m^3
Absorption coefficient	7.640 mm^{-1}	7.758 mm^{-1}
$F(0\,0\,0)$	792	1532
Final R indices $[I>2\sigma(I)]$	$R_1 = 0.0316$, w$R_2 = 0.0695$	$R_1 = 0.0281$, w$R_2 = 0.0582$
Largest diff. peak and hole	0.851 e Å^{-3} and 1.497 e Å^{-3}	0.834 e Å^{-3} and -1.217 e Å^{-3}

Among four oxygen atoms are from the four bridged 5-Brnic groups (O(1), O(2), O(5) and O(6) for Tb(1)) with the bond distances of 2.300(3)–2.360(3) Å between the Tb ion and oxygen atoms, and one oxygen atom is from one chelated 5-Brnic anion (O(4) for Tb(1)), whose bond distance is longer, 2.452(3) Å. Besides this, there exist another three oxygen atoms from the three coordinated water molecules (O(7), O(8) and O(9) for Tb(1)) with the bond distances of 2.391(3)–2.446(3) Å between the Tb ion and oxygen atoms. The bond average of Tb(1)–O distance is 2.381 Å. The bond angle consisting of Tb and the oxygen atoms ranges in 69.15(12)° (O(1)–Tb(1)–O(7))∼147.88(11)° (O(1)–Tb(1)–O(6)). Selected bond distances and bond angles for the chain-like terbium coordination polymer are listed in Table 2.

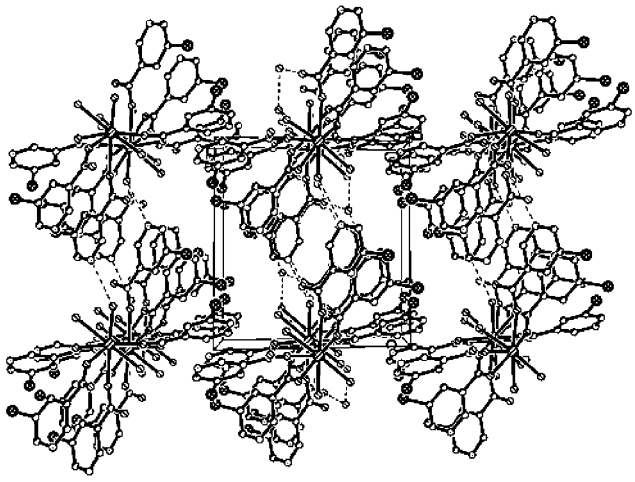

Fig. 2. Packing view of the unit cell for $\{[Tb(5\text{-Brnic})_3(H_2O)_3]\cdot H_2O\}_n$ coordination polymer.

All 5-Brnic anions are deprotonated, and there are two types of coordination modes of 5-Brnic anions existing in the molecular structure of the terbium 1-D coordination polymer: (1) bidentates bridging, all the oxygen atoms take part in the coordination to two central metal ions, connecting Tb ions to form the chain-like structure by this coordination mode. (2) monodentate chelating, the deprotonated oxygen atom coordinated to Tb ion. To our knowledge, this coordination mode is seldom seen in the structure of lanthanide complexes with nicotinic acid, most lanthanide nicotinic acid complexes that have been reported exist the bidentates chelation mode. Because only one oxygen atom connects to the central Tb ions, the unit of complex **2** has three coordinated water molecules, which is different from other complexes with only two coordinated water molecules [9–15].

Fig. 2 shows the packing view of a unit cell for complex **2**. The existence of water molecules causes the hydrogen bonding to all the nitrogen atoms of 5-Brnic anions, and there exist three types of O–H···N intermolecular hydrogen bonds: one is the O–H···N intermolecular hydrogen bonding between the nitrogen atoms of the bridged 5-Brnic anions and the oxygen atoms of the coordinated water molecules, whose bond angles is 154(5)° (O(8)–H(8A)···N(1)^{g}); the second is the O–H···N intermolecular hydrogen bonding between the nitrogen atoms of the chelated 5-Brnic anions and the oxygen atoms of the coordinated water molecules, whose angle is 155(5)° (O(7)–H(7B)···N(2)^{f}); the third is the O–H···N intermolecular hydrogen bonding between the nitrogen atoms of the chelated 5-Brnic anions and

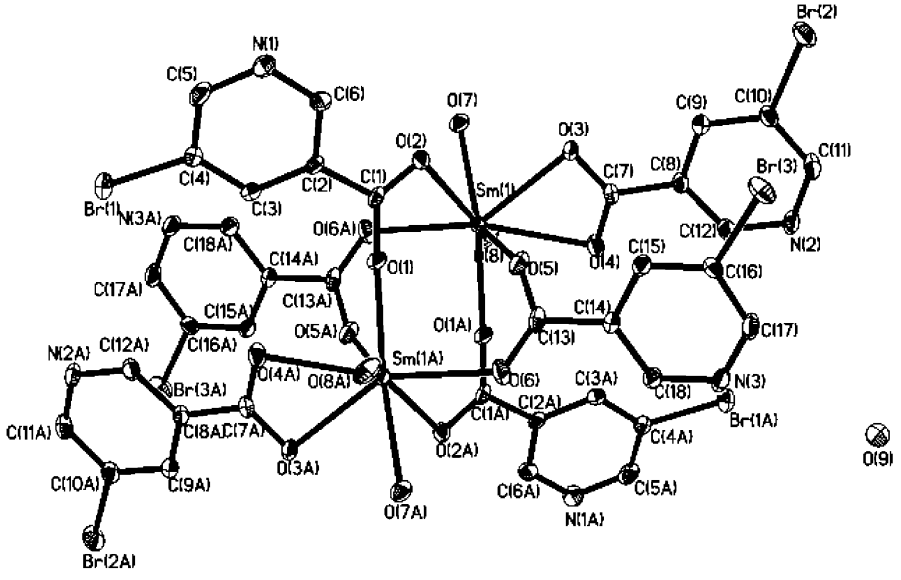

Fig. 3. Molecular structure of dimeric $[Sm(5\text{-Brnic})_3(H_2O)_2\cdot H_2O]_2$ complex.

Table 2
Selected bond distances (Å) and bond angles (°) for $\{[Tb(5\text{-Brnic})_3(H_2O)_3]\cdot H_2O\}_n$

Tb(1)–(1)	2.300(3)	Tb(1)–(7)	2.391(3)
Tb(1)–O(6)	2.330(3)	Tb(1)–O(8)	2.425(4)
Tb(1)–O(2)[a]	2.342(3)	Tb(1)–O(9)	2.446(3)
Tb(1)–O(5)[b]	2.360(3)	Tb(1)–O(4)	2.452(3)
O(1)–Tb(1)–O(6)	147.88(11)	O(7)–Tb(1)–O(8)	72.36(13)
O(1)–Tb(1)–O(2)[a]	105.01(11)	O(1)–Tb(1)–O(9)	76.94(11)
O(6)–Tb(1)–O(2)[a]	90.36(11)	O(6)–Tb(1)–O(9)	74.05(11)
O(1)–Tb(1)–O(5)[b]	95.70(12)	O(2)[a]–Tb(1)–O(9)	143.03(12)
O(6)–Tb(1)–O(5)[b]	88.09(11)	O(5))–Tb(1)–O(9)	71.69(11)
O(2)[a]–Tb(1)–O(5)[b]	142.47(11)	O(7)–Tb(1)–O(9)	131.89(12)
O(1)–Tb(1)–O(7)	69.15(12)	O(8)–Tb(1)–O(9)	130.53(13)
O(6)–Tb(1)–O(7)	142.40(12)	O(1)–Tb(1)–O(4)	79.20(11)
O(2)[a]–Tb(1)–O(7)	79.97(13)	O(6)–Tb(1)–O(4)	79.51(11)
O(5)[b]–Tb(1)–O(7)	78.68(12)	O(2)[a]–Tb(1)–O(4)	71.02(11)
O(1)–Tb(1)–O(8)	141.42(13)	O(5)[b])–Tb(1)–O(4)	144.79(10)
O(6)–Tb(1)–O(8)	70.18(12)	O(7)–Tb(1)–O(4)	129.26(11)
O(2)[a]–Tb(1)–O(8)	70.21(13)	O(8)–Tb(1)–O(4)	129.83(12)
O(5)[b]–Tb(1)–O(8)	74.05(13)	O(9)–Tb(1)–O(4)	73.23(11)

For symmetry transformations used to generate equivalent atoms: [a]: $-x, -y, -z+2$; [b]: $-x, -y+1, -z+2$.

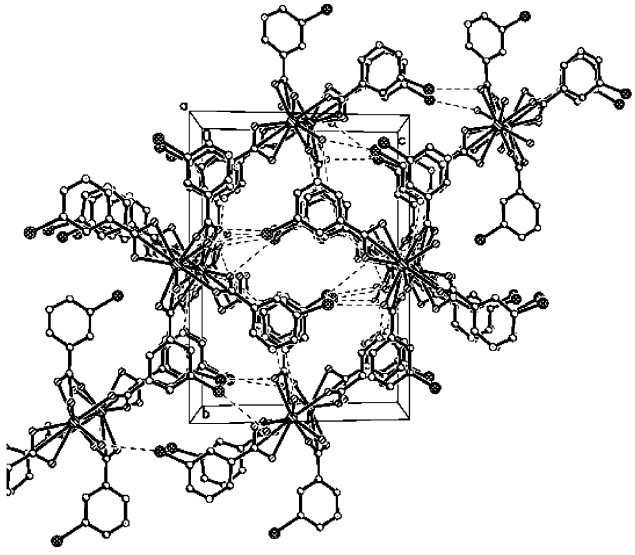

Fig. 4. Packing view of the unit cell for $[Sm(5\text{-Brnic})_3(H_2O)_2\cdot H_2O]_2$ complex.

the oxygen atoms of the lattice water molecules, whose angle is 133(5)° (O(10)–H(10A)···N(3)). Besides these O–H···N hydrogen bonding, there also exist two types of O–H···O intermolecular hydrogen bonds: one is the O···H–O intermolecular hydrogen bonding between the oxygen atoms of the bridged 5-Brnic anions and the oxygen atoms of the coordinated water molecules, whose bond angle is 158(10)° (O(7)–H(7A)···O(4)^d); the other is the O···H–O intermolecular hydrogen bonding between the oxygen atom of coordinated water molecules and the oxygen atom of the crystal water molecules, whose bond angle is 159(5)° (O(8)–H(8B)··· O(10)^f). All these intermolecular hydrogen bonding link up the complex units, resulting in a 3-D network and leading the whole network structure system stable. The detailed data of hydrogen bonding are shown in Table 4.

Fig. 3 and Table 1 give the coordination geometry and atom labeling in the crystal structure of complex **3**. XRD crystal structure analysis reveals that it leads to a dimer-like formulation $[Sm(5\text{-Brnic})_3(H_2O)_2\cdot H_2O]_2$ with two equivalent structural units corresponded to one half of dimer related by a crystallographic inversion center, which is similar with $Sm_2(C_5H_4NCO_2)(H_2O)_4$ [15]. There exists only one metal coordination environment in the molecular structure, i.e., the two symmetrical samarium ions are bridged by four 5-Brnic anions. Each central samarium ion belongs to be eight-coordinated, whose coordination geometry can be described as a distorted square antiprism geometry. Among four oxygen atoms are from the four bridged 5-Brnic anions (O(1), O(2), O(5) and O(6) for Sm(1)) with the bond distances of 2.343(3)–2.485(3) Å between the Sm ion and oxygen atoms, and two oxygen atoms are from the chelated 5-Brnic anions (O(3) and O(4) for Sm(1)), whose bond distances are longer, 2.490(3) Å (Sm(1)–O(3)) and 2.544(3) Å (Sm(1)–O(4)), respectively. The bond distances of Sm and oxygen atoms which from 5-Brnic anions are shorter than Sm–O of $Sm_2(C_5H_4NCO_2)(H_2O)_4$, which indicates that the existence of Br atom weaken the attraction between phenyl cycle and carboxylate ions and resulting the strengthening of the interaction of COO- and Sm ion. In addition, there exist another two coordinated oxygen atoms from two water molecules (O(7) and O(8) for Sm(1)) with the bond distances are 2.428(3) Å (Sm(1)–O(7)) and 2.429(3) Å (Sm(1)–O(8)) between the Sm ion and oxygen

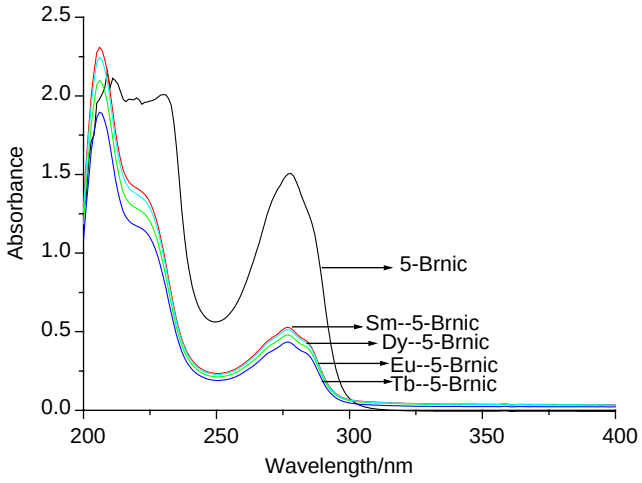

Fig. 5. Ultraviolet absorption spectra of Lanthanide complexes of 5-Brnic (*Ln* = Tb, Gd, Sm).

atoms. The average bond Sm(1)–O distance is 2.438 Å, much longer than complex **1**, which is probably due to the radius of Sm ions is longer than Tb ions. The bond angle consisting of Sm and the oxygen atoms of chelated 5-Brnic anion is 51.81(9)° (O(3)–Sm(1)–O(4)). Selected bond distances and bond angles for the dimeric samarium complex are listed in Table 3.

All 5-Brnic anions are deprotonated and all the oxygen atoms take part in the coordination to the two central metal ion. There are two types of coordination modes of 5-Brnic anions existing in the molecular structure: (1) bidentates bridging, two Sm ions are connected into dimeric structure by this coordination mode. (2) bidentates chelation, both two oxygen atoms of the carboxyl group coordinated to Sm ion, which is different from the coordination mode of complex **2**.

Fig. 4 shows the packing view of a unit cell for dimeric complex **3**. According to the diagram, two types of O–H···N intermolecular hydrogen existing in the structure: one is the O–H···N between the nitrogen atoms of the bridged 5-Brnic anions and the oxygen atoms of the coordinated water molecules (O(9)–H(9A)···N(1) and O(8)–H(8B)···N(3)^{m})), another is the O–H···N between the nitrogen atoms of the chelated 5-Brnic anions and the oxygen atoms of the crystal water molecules (O(7)–H(7A)···N(2)^{l})). In addition, there exist the O–H···O intermolecular hydrogen bonds between the oxygen atoms of coordinated water molecules and the oxygen atoms of the lattice water molecules (O(9)–H(9B)···O(7)^{i}), O(9)–H(9B)···O(8)^{j}), O(7)–H(7B)···O(9)^{m}) and O(8)–H(8A)…O(9)^{m})). All intermolecular hydrogen bonds result in a 3-D network and lead the whole network structure system stable. The detailed data of hydrogen bonding is also shown in Table 4.

Table 3
Selected bond distances (Å) and bond angles (°) for [Sm(5-Brnic)$_3$(H$_2$O)$_2$ · H$_2$O]$_2$

Sm(1)–O(1)^{c}	2.343(3)	Sm(1)–O(8)	2.429(3)
Sm(1)–O(5)	2.367(3)	Sm(1)–O(6)^{c}	2.485(3)
Sm(1)–O(2)	2.417(3)	Sm(1)–O(3)	2.490(3)
Sm(1)–O(7)	2.428(3)	Sm(1)–O(4)	2.544(3)
O(1)^{c}–Sm(1)–O(5)	73.47(11)	O(8)–Sm(1)–O(6)^{c}	76.51(11)
O(1)^{c}–Sm(1)–O(2)	126.97(11)	O(1)^{c}–Sm(1)–O(3)	125.88(9)
O(5)–Sm(1)–O(2)	73.90(10)	O(5)–Sm(1)–O(3)	77.01(11)
O(1)^{c}–Sm(1)–O(7)	150.62(11)	O(2)–Sm(1)–O(3)	84.82(9)
O(5)–Sm(1)–O(7)	135.71(11)	O(7)–Sm(1)–O(3)	69.75(10)
O(2)–Sm(1)–O(7)	74.71(11)	O(8)–Sm(1)–O(3)	101.07(12)
O(1)^{c}–Sm(1)–O(8)	79.19(12)	O(6)^{c}–Sm(1)–O(3)	145.49(10)
O(5)–Sm(1)–O(8)	143.56(11)	O(1)^{c}–Sm(1)–O(4)	76.59(10)
O(2)–Sm(1)–O(8)	142.53(11)	O(5)–Sm(1)–O(4)	73.61(10)
O(7)–Sm(1)–O(8)	72.94(12)	O(2)–Sm(1)–O(4)	130.31(9)
O(1)^{c}–Sm(1)–O(6)^{c}	87.93(10)	O(7)–Sm(1)–O(4)	105.39(11)
O(5)–Sm(1)–O(6)^{c}	125.14(11)	O(8)–Sm(1)–O(4)	77.00(11)
O(2)–Sm(1)–O(6)^{c}	78.19(9)	O(6)^{c}–Sm(1)–O(4)	151.36(9)
O(7)–Sm(1)–O(6)^{c}	76.84(11)	O(3)–Sm(1)–O(4)	51.81(9)

For symmetry transformations used to generate equivalent atoms: ^{c}: $-x, -y, -z+2$.

Table 4
Hydrogen bonds (Å) for {[Tb(5-Brnic)$_3$(H$_2$O)$_3$] · H$_2$O}$_n$ (1) and [Sm(5-Brnic)$_3$(H$_2$O)$_2$ · H$_2$O]$_2$ (2)

D–H…A	d(D–H)	d(H…A)	d(D…A)	d(DHA)
(1)				
O(7)–H(7A)…O(4)^{d}	0.84(2)	2.07(4)	2.866(5)	158(10)
O(7)–H(7B)…N(2)^{e}	0.839(19)	2.06(3)	2.845(5)	155(5)
O(8)–H(8A)…N(1)^{f}	0.815(19)	2.29(3)	3.042(6)	154(5)
O(8)–H(8B)…O(10)^{g}	0.823(19)	1.82(3)	2.605(7)	159(5)
O(10)–H(10A)…N(3)	0.838(19)	2.16(5)	2.803(7)	133(5)
(2)				
O(9)–H(9B)…O(7)^{i}	0.84(2)	2.28(12)	2.715(5)	113(10)
O(9)–H(9B)…O(8)^{j}	0.84(2)	2.11(6)	2.829(5)	144(9)
O(9)–H(9A)…N(1)^{k}	0.821(19)	2.06(3)	2.825(5)	154(6)
O(7)–H(7A)…N(2)^{l}	0.84(2)	1.90(2)	2.734(4)	170(7)
O(8)–H(8B)…N(3)^{m}	0.847(19)	2.01(3)	2.792(5)	154(6)
O(7)–H(7B)…O(9)^{m}	0.820(19)	1.91(2)	2.715(5)	165(5)
O(8)–H(8A)…O(9)^{m}	0.814(19)	2.06(3)	2.829(5)	158(5)

For symmetry transformations used to generate equivalent atoms. For complex **1**: ^{d}: $-x+1, -y+1, -z+2$; ^{e}: $-x, -y+1, -z+2$; ^{f}: $x, y, z+1$; ^{g}: $x, y-1, z$. For complex **2**: ^{i}: $-x+1, -y, -z+1$; ^{j}: $x-1/2, -y+1/2, z-1/2$; ^{k}: $x, y+1, z$; ^{l}: $-x+3/2, y-1/2, -z+1/2$; ^{m}: $x+1/2, -y+1/2, z+1/2$.

3.2. Photophysical properties

Fig. 5 shows ultraviolet-visible absorption spectra for free 5-Brnic ligand and its lanthanide (Eu, Tb, Sm, Dy) complexes (**1**, **2**, **3**, **4**) (10^{-4} mol L^{-1} ethanol solution). They all exhibit domain absorption peaks in the narrow ultraviolet region in the range of 200–300 nm and the

maximum absorption peaks locate at around 277 nm, which can be attributed to the characteristic absorption of 5-Brnic. Besides this, the characteristic absorption band belonging to phenyl cycle for the four complexes exhibit at about 209 nm and a little blue shift compared with that of 5-Brnic, suggesting that coordination interaction between lanthanide ions and 5-Brnic to form the more extensive $\pi \rightarrow \pi^*$ conjugated system. The results indicate that 5-Brnic is the energy donor and luminescence sensitizer of Ln^{3+} ion.

The phosphorescence spectrum of the corresponding gadolinium complex (**5**) was measured owing to its high phosphorescence–fluorescence ratio compared to those of the other Ln^{3+} complexes and Gd^{3+} can sensitize the phosphorescence emission of ligands. (as shown in Fig. 6). From the phosphorescence emission, three apparent phosphorescence bands appear and the maximum phosphorescence wavelengths are at 411, 431 and 457 nm, respectively, which are attributed to the characteristic 0–0 transition, 0–1 transition and 0–2 transition of 5-Brnic ligand. From the shortest wavelength of the phosphorescence emission band corresponed to be the 0–0 transition, the lowest triplet state energy of 5-Brnic can be determined to be 24 330 cm^{-1}. The energy differences between it and the emitting levels of Ln^{3+} (Ln = Sm, Eu, Tb, Dy) were calculated, the data are shown in Table 5.

According to Sato's result [19], the intramolecular energy migration efficiency from organic ligands to the central Ln^{3+} is the most important factor influencing the luminescence properties of rare earth complexes. The intramolecular energy transfer efficiency depends mainly on the two energy transfer processes [20]. One is from the lowest triplet state energy of organic to the resonant energy level by Dexter's resonant exchange

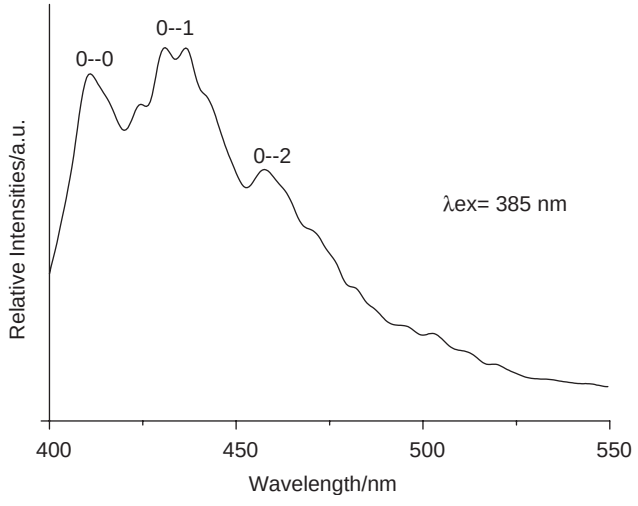

Fig. 6. Phosphorescence spectrum of $Gd(5\text{-Brnic})_3(H_2O)_3$ complex.

Table 5
The lowest triplet energy of Gd^{3+} complex with 5-Brnic and the energy difference

Ln^{3+}	Lowest triplet state energy (Tr) (cm^{-1})	ΔE(Tr–Ln^{3+}) (cm^{-1})
Eu^{3+}	24 330	7065
Tb^{3+}	24 330	3930
Sm^{3+}	24 330	7580
Dy^{3+}	24 330	3455

Ln^{3+}: Eu^{3+}, $^5D_0$ (17 265 cm^{-1}); Tb^{3+}, $^5D_4$ (20 500 cm^{-1}); Sm^{3+}, $^4G_{5/2}$ (17 900 cm^{-1}); Dy^{3+}, $^4F_{9/2}$ (20 875 cm^{-1}).

interaction theory [21]:

$$k_{ET} = KP_{da}\ \exp(-R_{da}/L), \quad (1)$$

$$P_{da} = (2\pi Z^2/R)\int F_d(E)E_a(E)\,dE, \quad (2)$$

$$k_{ET} = KP_{da}\exp(-2R_{da}/L) = K\int F_d(E)E_a(E)\,dE, \quad (3)$$

The other is the inverse energy transition by the thermal deactivation mechanism [22]:

$$k(T) = A\exp(-\Delta E/RT), \quad (4)$$

where k_{ET} is the rate constant of the intermolecular energy transfer and P_{da} is the transition probability of the resonant exchange interaction. $2\pi Z^2/R$ is the constant relating to the specific mutual distance between the central Ln^{3+} ion and its coordinated atoms (O or N). $F_d(E)$ and $E_a(E)$ are the experimental luminescence spectrum of energy donor (ligands) and the experimental absorption spectrum of energy acceptor (Ln^{3+}) respectively, so both of them represent the overlap spectrum of Ln^{3+}. R_{da} is the intermolecular distance between donor atoms and acceptor atoms, and L is the van der waals radius. Both R_{da} and L may be considered to be constant in intramolecular transfer processes, so k_{ET} is proportional to the overlap of $F_d(E)$ and $E_a(E)$. With the decrease in the energy difference between the triplet state energy of conjugated carboxylic acid and Ln^{3+}, the overlap of $F_d(E)$ and $E_a(E)$ is increased. So from the above equation, it can be concluded that the less the overlap between the luminescence spectrum of organic ligands and the emissive energy of Ln^{3+}, the more the intramolecular energy rate constant k_{ET}. On the other hand, the activation energy ΔE in Eq. (4) is equal to the energy difference $\Delta E(\mathrm{Tr}-Ln^{3+})$, while from the formula, the inverse energy transfer rate constant $k(T)$ increased with decreasing $\Delta E(\mathrm{Tr}-Ln^{3+})$ [23–25].

As discussed above, there should exist an optimal energy difference between the triplet position of 5-Brnic and the emissive energy level Ln^{3+}, the larger and the smaller $\Delta E(\mathrm{Tr}-Ln^{3+})$ will decrease the luminescence

properties of rare earth complexes. In Table 5, the energy differences for Tb^{3+} and Dy^{3+} are smaller than those for Sm^{3+} and Eu^{3+}. So it can be predicted that the triplet state energy of 5-Brnic is more suitable for the luminescence of Tb^{3+} and Dy^{3+} than Sm^{3+} and Eu^{3+}. In addition, there exist a lot of internal energy level ($^6F_{11/2}$, $^6F_{9/2}$,…,$^6H_{11/2}$ etc) between the first excited state $^4G_{5/2}$ and ground state $^6H_{9/2}$ of Sm^{3+}, which causes readily some non-radiative energy transfer process to loss the excited energy of 5-Brnic. So Sm^{3+} complex exhibits the weakest luminescence.

The excitation spectra of these lanthanide complexes (solid samples) show that the effective energy absorption mainly take place in the narrow ultraviolet region of 200–290 nm, and the dysprosium complex has effective absorption in long wavelength ultraviolet region of the range 300–350 nm, moreover (Inner plot of Figs. 7–10). The excitation bands of complex **1** under the red emission of 613 nm possess two main peaks, 221 and 242 nm, respectively. The excitation bands for complex **2** under the green emission of 543 nm shows five main peaks, 222.5, 240, 259, 271.5 and 290 nm, respectively. The excitation band for of complex **3** under the orange emission of 596 nm shows one main peak with the maximum excitation wavelengths at 246 nm. The excitation bands for the complex **4** under the blue emission of 484 nm possess seven main peaks, 240, 259, 271, 283, 292, 308 and 330 nm, respectively.

We further measured the corresponding emission spectra by selectively excitation with the different excitation wavelengths of the above four complexes, and they show the similar emission position except for little distinction of luminescent intensities. Which indicate that the excitation bands are all the effective energy sensitizer for the luminescence of *Ln* ions. The emission spectra were shown in the outer plot of

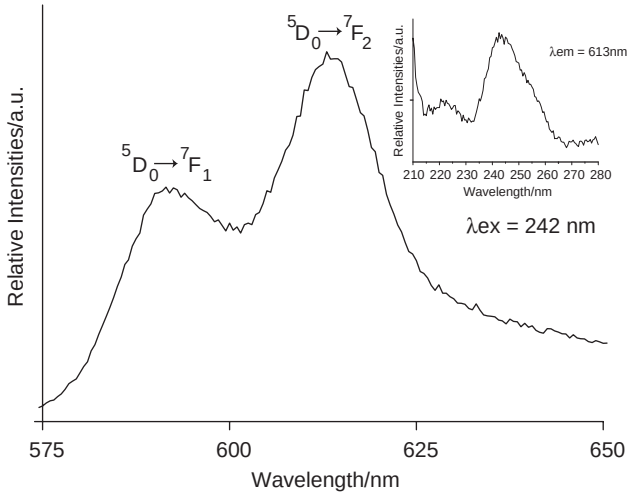

Fig. 7. Luminescent spectra of $Eu(5\text{-Brnic})_3(H_2O)_3$ complex: outer plot for emission spectrum and inner plot for excitation spectrum.

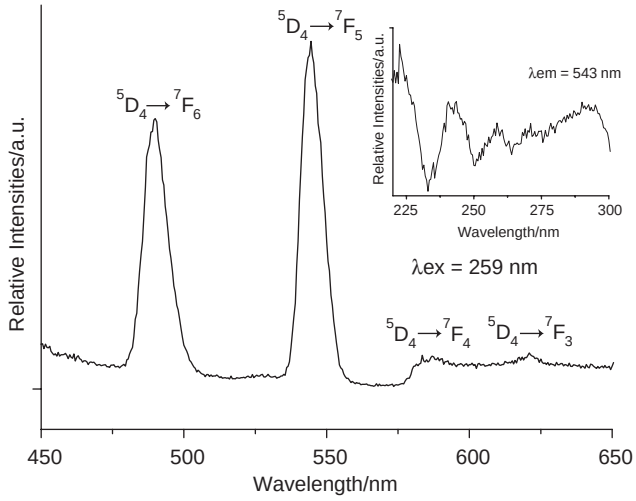

Fig. 8. Luminescent spectra of $\{[Tb(5\text{-Brnic})_3(H_2O)_3]\cdot H_2O\}_n$ complex: outer plot for emission spectrum and inner plot for excitation spectrum.

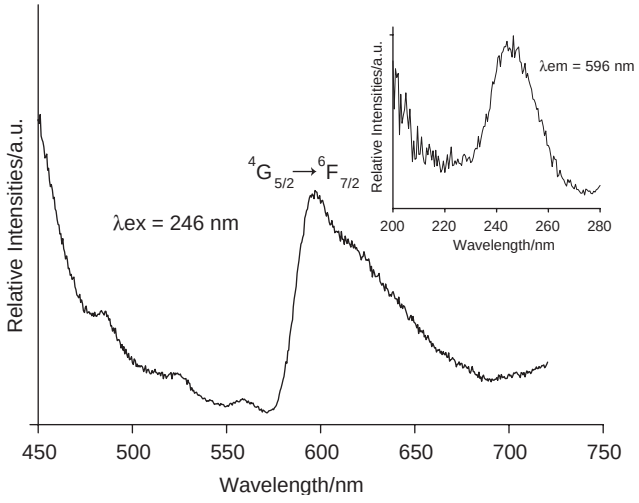

Fig. 9. Luminescent spectra of $[Sm(5\text{-Brnic})_3(H_2O)_2\cdot H_2O]_2$ complex: outer plot for emission spectrum and inner plot for excitation spectrum.

Figs. 7–10. For complex **1**, the emission spectra show two emission peaks under the excitation of 242 nm: 591 nm and 613 nm, corresponded to the characteristic emission $^5D_0 \rightarrow {}^7F_J$ transitions ($J = 1, 2$) of Eu^{3+} ion. Among the red luminescent intensity of $^5D_0 \rightarrow {}^7F_2$ transition is the strongest, and the emission intensity of $^5D_0 \rightarrow {}^7F_1$ transition becomes stronger for the overlap of $^5D_0 \rightarrow {}^7F_0$ transition. For complex **2**, the emission spectra show four emission peaks under the excitation of 259 nm: 490 nm, 543 nm, 583 nm and 620 nm, attributed to be the characteristic emission $^5D_4 \rightarrow {}^7F_J$ ($J = 6, 5, 4, 3$) transition of Tb^{3+} ion. Among the $^5D_4 \rightarrow {}^7F_5$ transition exhibits the strongest green emission, and

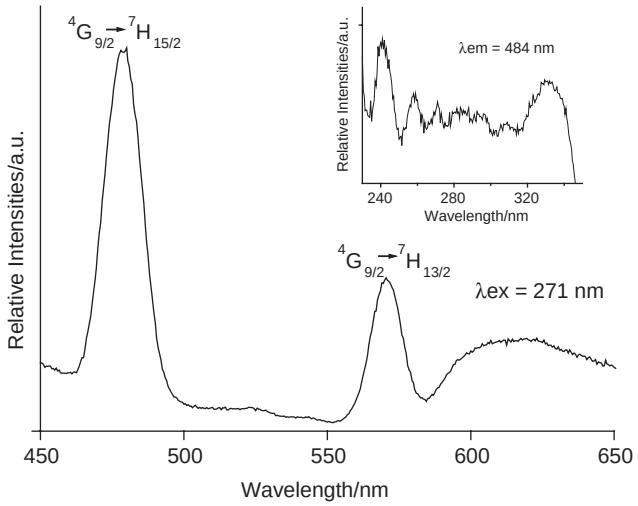

Fig. 10. Luminescent spectra of $Dy(5\text{-Brnic})_3(H_2O)_3$ complex: outer plot for emission spectrum and inner plot for excitation spectrum.

$^5D_4 \rightarrow {}^7F_6$ transition shows the second strongest blue emission. For complex **3**, the emission spectra show one emission peaks under the excitation of 246 nm and the maximum emission wavelengths are at 597 nm, which attributed to be the characteristic emission $^4G_{5/2} \rightarrow {}^6H_J$ ($J = 7/2$) transition of Sm^{3+} ion. For complex **4**, the luminescence spectrum shows two apparent emission peaks under the excitation of 271 nm: one is at 480 nm, the other is at 570 nm, which is corresponded with be the characteristic emission $^4F_{9/2} \rightarrow {}^6H_J$ ($J = 15/2,\ 13/2$) transition of Dy^{3+} ion. It is worthy pointing out that the blue emission intensity of $^4F_{9/2} \rightarrow {}^6H_{15/2}$ transition is stronger than the yellow emission of $^4F_{9/2} \rightarrow {}^6H_{13/2}$, suggesting that 5-Brnic is more suitable for the sensitization of blue luminescence of Dy^{3+}.

Comparing the luminescence intensities of these complexes under the same maximum excitation, it can be found that complex **2** and complex **4** show the stronger luminescence than those of complex **1** and complex **3**. The samarium and europium complexes show much weaker luminescence than terbium complex and dysprosium ones. Which takes agreement with the prediction from the energy transfer mechanism.

4. Conclusions

In summary, under the same reaction conditions and with similar reactants, five lanthanide (Eu (**1**), Tb (**2**), Sm (**3**), Dy (**4**), Gd (**5**)) complexes with 5-Brnic have been synthesized and characterized. The X-ray analysis reveals that different lanthanide complex has different structure. The complex **2** has a one-dimension chain-like polymeric structure while complex **3** has a dimeric molecular structure. The triplet state energy of 5-Brnic is determined to be 24 330 cm^{-1} with the 0–0 transition in the phosphorescence spectrum of the gadolinium complex at about 411 nm. The energy match energy transfer processes between 5-Brnic and lanthanide ions (Eu^{3+}, Tb^{3+}, Sm^{3+}, Dy^{3+}) have been studied, predicting the more optimum energy transfer between 5-Brnic and Tb^{3+} or Dy^{3+} than Eu^{3+} or Sm^{3+}, and resulting the stronger luminescence of terbium and dysprosium complexes.

Acknowledgment

The work was supported by the National Natural Science Foundation of China (20301013).

Supplementary materials

Crystallographic data (excluding structure factors) for the structure reported in this paper have been deposited with the Cambridge Crystallographic Data Centre as supplementary publication no. CCDC—228522 (complex Sm_2) and CCDC—228523 (complex Tb_n). Copies of the data can be obtained free of charge on application to CCDC, 12 Union Road, Cambridge CB21EZ, UK (Fax: +44-1223-336-033; E-mail: deposit@ccdc.cam.ac.uk).

References

[1] B. Yan, H.-J. Zhang, S.-B. Wang, J.-Z. Ni, Mater. Chem. Phys. 52 (1997) 151.
[2] B. Yan, H.-J. Zhang, S.-B. Wang, J.-Z. Ni, Mater. Res. Bull. 33 (1998) 1511.
[3] Y.-X. Ci, Y.-Z. Li, W.-B. Chang, Anal. Chim. Acta 248 (1992) 589.
[4] L.K. Scott, W.D. Horrocks, J. Inorg. Biochem. 46 (1992) 193.
[5] L.-P. Jin, S.-X. Lu, S.-Z. Lu, Polyhedron 15 (1996) 4069.
[6] W.M. Xue, Q.G. Wang, L. Yan, R.D. Yang, Polyhedron 11 (1992) 2051.
[7] E.P. Marinho, D.M. Araujo Melo, L.B. Zinner, K. Zinner, E.E. Castellano, J. Zukerman-Schpector, P.C. Isolani, G. Vicentini, Polyhedron 16 (1997) 3519.
[8] D.T. Vodak, M.E. Braun, J. Kim, M. Eddaoudi, O.M. Yaghi, Chem. Commun. (2001) 2534.
[9] R.A. Chupakhina, V.V. Serebrennikov, Russ. J. Inorg. Chem. (1963) 665.
[10] R.A. Chupakhina, E.N. Korableva, V.V. Serebrennikov, Russ. J. Inorg. Chem. (1966) 427.
[11] B. Yan, Q.-Y. Xie, Inorg. Chem. Commun. 6 (2003) 1448.
[12] B. Yan, Q.-Y. Xie, J. Mol. Struct. 688 (2004) 73.
[13] R.A. Chupakhina, V.V. Serebrennikov, Russ. J. Inorg. Chem. (1962) 1406.
[14] J. Kay, J.W. Moore, M.D. Glick, Inorg. Chem. 11 (1972) 2825.
[15] J.W. Moore, M.D. Glick, W.A. Baker, J. Am. Chem. Soc. 94 (1972) 1858.
[16] J.-J. An, Z.-C. Chen, Translation of Handbook on the Synthesis of Inorganic Compounds, vol. II, Chemical Society of Japan, 1986, p. 261.
[17] G.M. Sheldrick, Acta Crys. A 46 (1990) 467.
[18] G.M. Sheldrick, SHELXS-97, a Program for X-ray Crystal Structure Solution, and SHELXL-97, a Program for X-ray Structure Refinement, Gottingen University, Germany, 1997.

[19] S. Sato, M. Wada, Bull. Chem. Soc. Japan 43 (1970) 1955.
[20] S.-L. Wu, Y.-L. Wu, Y.-S. Yang, J. Alloys Compd. 180 (1994) 399.
[21] D.L. Dexter, J. Chem. Phys. 21 (1953) 836.
[22] T.D. Brown, T.M. Shepherd, J. Chem. Soc. Dalton Trans. (1973) 336.
[23] H.-J. Zhang, B. Yan, S.-B. Wang, J.-Z. Ni, J. Photochem. Photobiol. A: Chem. 109 (1998) 223.
[24] B. Yan, H.-J. Zhang, S.-B. Wang, J.-Z. Ni, Spectrosc. Lett. 31 (1998) 603.
[25] B. Yan, H.-J. Zhang, S.-B. Wang, J.-Z. Ni, Monatsh. Chem 129 (1998) 567.